scientific reports

Check for updates

OPEN

Enhancement the stability of the titanium/graphite photo-electrode in varying voltages for treatment of textile wastewater using reactive blue 19 as the model contaminant

Mahboobeh Dehvari[1,2], Behzad Jamshidi[1,3], Bazieva Aliia Mansurovna[4], Ali Akbar Babaei[1,2] & Sahand Jorfi[1,2]✉

This study aims to investigate the treatment of textile wastewater containing reactive blue 19 dye (RB19) by graphite-based photo-electrode (GBPE). Simultaneously with the electrocatalytic process, irradiation by UVA lamp was also performed. The residual dye concentration was measured by UV/Visible spectrophotometry at wavelength of 590 nm. The structural characteristics of the composite was analyzed using FESEM, FTIR, and XRD. According to the results, the highest removal efficiency was obtained under acidic pH conditions. The maximum removal of 100% of the dye was observed in the different voltages and times (1.5 V/cm at 120 min, 2 V/cm at 100 min and 2.5 and 3 V/cm at 80 min). Under optimal conditions of pH = 5, RB19 concentration 100 mg/L, time of 20 min, voltage 0. 5 V/cm, and UVA irradiation of 12 W, the removal efficiency was 33%. The loose of graphite electrode (GE) duo to corrosion was 1 g in UVA/TiO_2/EK which increased to 2.1 g in UVA/EK. The removal efficiency of RB19 after six runs decreased to 63%. Results of oxygen consumption rate inhibition (OCRI) test showed the highest decrease in toxicity for the EK process, while the UVA/TNPs/EK process exhibited the least reduction. The real wastewater treatment using electrolysis with GBPE showed the removal efficiencies of 32% and 40% for COD and TOC, respectively. The findings provide valuable insights into the efficiency of titanium/graphite photo-electrodes for textile wastewater treatment applications.

Keywords TiO_2/graphite, Photo-electrode, Electrode stability, Textile wastewater, Reactive blue 19

The textile industry is considered one of the most important industrial sectors in developing countries. These industries produce wastewater with highly variable characteristics[1,2]. Textile wastewater contains significant amounts of dye compounds, which are typically toxic, resistant to biological degradation, and environmentally persistent[3]. The discharge of textile wastewater into water bodies leads to adverse effects, such as ecological disruption, eutrophication, reduced photosynthesis, and overall environmental damage. Consequently, this wastewater is recognized as an environmental threat and must be treated before being released into the environment. Textile dyes have mutagenic and carcinogenic effects on human health[3,4].

The conventional methods used for treating wastewater from the textile industry include physical, chemical, and biological methods. Given the significant quality fluctuations in the wastewater from these industries, most conventional methods often do not perform satisfactorily[5,6]. Due to the low biodegradability of dye compounds, physicochemical treatment methods have gained more acceptance compared to biological methods[7]. Common physicochemical methods such as electrochemical treatment, coagulation, ozonation, chemical precipitation, Fenton, photo-Fenton, reverse osmosis, ion exchange, ultraviolet radiation, and adsorption process, have been used to remove dyes from textile wastewater[8–10]. Each of these technologies has its limitations. Advanced oxidation processes (AOPs), given their high efficiency in color removal and significant advancements in recent decades, have gained considerable importance in the treatment of industrial effluents[11,12]. Both homogeneous

[1]Environmental Technologies Research Center, Medical Basic Sciences Research Institute, Ahvaz Jundishapur University of Medical Sciences, Ahvaz, Iran. [2]Department of Environmental Health Engineering, School of Public Health, Ahvaz Jundishapur University of Medical Sciences, Ahvaz, Iran. [3]Department of Environmental Health Engineering, Petroleum Industry Health Organization, NIOC, Ahvaz, Iran. [4]Osh State University, Osh, Kyrgyzstan. ✉email: sahand369@yahoo.com

and heterogeneous AOPs have been highly effective in degrading-colored compounds by the destructive oxidation of the dyes. Photocatalytic method is highly effective in the degradation of organic pollutants[13,14].

The photocatalytic process is a chemical reaction facilitated by a photocatalyst, typically under light irradiation, that accelerates the breakdown of organic pollutants into non-toxic substances. Metal oxides perform well as photocatalysts in various applications, but scientific studies have shown that titanium dioxide (TiO_2) has more advantages than others including being active in the ultraviolet (UV) region, non- toxicity, low cost, availability and chemical stability. Due to the high energy required by TiO2 for its bandgap (3.2–3.5 eV), it requires UV light which provides the necessary energy[13,15–17].

In many cases, the separating photocatalyst nanaoparticles from the solution requires additional cost and time. Besides, the complete separation of these nanoparticles is not feasible and as a result, incomplete separation leads to the formation of secondary pollutants in the solution. Therefore, an effective solution to prevent this problem is to immobilize the photocatalyst nanoparticles on suitable substrates[18–20].

Graphite has a layered structure composed of carbon clusters called graphene. Using graphite sheets and stabilizing titanium dioxide nanoparticles (TiO_2) on them is one of the effective methods to improve photocatalytic performance in order to remove dyes from wastewater. Graphite sheets have very good electrical conductivity and high surface area. This leads to an increase in the number of active sites and thus increases the efficiency of the photocatalytic process[19,21,22].

Dyes are complex substances that enter the environment during various stages such as dyeing and finishing in the textile industry. Dye compounds are usually toxic, resistant to biological degradation, and environmentally persistent. A real wastewater of textile industry typically consists a mixture of dyes. In this study, Reactive Blue 19 (RB19) was used as the model contaminant.

This study aims to photodegrade RB19 from textile wastewater using TiO_2 nanoparticles immobilized on graphite electrode.

Material and methods

Materials

Analytical grade chemicals including nano-sized titanium dioxide 99.8%, mercuric sulfate 99.99%, hydroxide 99.8%, sulfuric acid 98% and silver sulfate 99.99% were purchased from Merck Co, Germany. Graphite based electrodes were prepared with dimensions of 20 cm × 4 cm × 1.5 cm from Zobeir Corporation, Iran. Reactive blue 19 ($C_{22}H_{16}N_2Na_2O_{11}S_3$) was obtained from Alvan-Sabet Inc, (Iran). The real textile wastewater was taken from Boujerd textile incorporation monthly, and transported to the laboratory in a cold box at 4 °C immediately. Textile wastewater characteristics are presented in Table 1.

The photo-reaction chamber

All photo-chemical reactions were carried out in a rectangular quartz-made chamber with a total volume of 1200 mL (6 cm × 20 cm × 10 cm) in which, 70% of total volume belonged to the reaction section. The light source for initiation of photo-reactions was supplied by a UVA lamp (12 W) with the length of 15 cm which was installed exactly close to one side of reaction chamber at the least possible distance of 2 cm. The surrounding space and personnel of the lab were protected against UV irradiation by covering the whole reactor with a wood box and aluminum foil. Graphite based electrodes were inserted into the photo-reactor chamber in a designed distance of 6 cm from each other. A laboratory DC power (Model: PS 303D, 30 V, 5 A) by the ability of adjusting voltage supplied the electric power through connection to the electrodes with wire. Before each experimental run, synthetic or real textile wastewater was prepared according to pre-determined characteristics. All experiments were triplicate and conducted at room temperature (28 ± 3 °C). After determination of selected level of each variable, a series of experiments were conducted using a real textile wastewater sample to simulate the real conditions on stability of photo-electrodes as well as organic matter removal. It should be noted that the initial COD was determined before any experimental run, to prevent any possible mistake in analysis results and findings.

The sequence of conducting experiments

One factor at the time methodology was considered for investigation of the effect of independent variables on the targeted response[23]. The removal of RB 19 and the weight of photo-electrode were investigated as the main dependent variables along with varying the levels of 6 independent variables including pH (3–9), voltage (0.5–3 V/cm), contact time (20–120 min), UVA intensity (4–12 W), TiO_2/graphite surface ratio in photo-electrode (level 1, level 2, level 3) and existence or absence of radical scavengers. The RB 19 concentration was kept constant in all experiments as 100 mg/L.

Characteristic	Value
COD (mg/L)	1284 ± 173
BOD_5 (mg/L)	398 ± 66
TOC (mg/L)	912 ± 97
TSS (mg/L)	188 ± 21
TDS (mg/L)	685 ± 176
pH	6.2–6.9

Table 1. Textile wastewater characteristics.

Preparation of graphite-based photo-electrode (GBPE)

The bare graphite (BG) sheets were immersed in a bare TiO_2 nanoparticles (BTN) suspension (50%) for 5 min and thereafter were removed and dried at 100 °C. The process of immersion and dryness of photo-electrodes was repeated five times.

Finally, the calcination of dried photo-electrodes was performed at 550 °C for another 2 h in a nitrogen furnace Field emission scanning electron spectrometry (FESEM-EDX, model Mira III, TESCAN, Czech Republic) was used the characterize the morphology synthetized photo-electrodes. The crystalline structures of synthetized photo-electrode were studied using the X-ray diffraction (XRD) analysis (Model: PW1730, Philips, Holland) in which Cu Kα radiation (λ = 1.54056 A) at tube voltage/current, 40 kV/30 mA within the 2θ scanning range of 10–80° was used. The functional groups of photo-electrode were determined by Fourier transform infrared spectroscopy (FTIR).

The point of zero charges (pH_{zpc}) of synthetized photo-electrode was calculated at the pH range of 2–12. The desired pH values were adjusted in a series of flasks using H_2SO_4 (0.5 M) and NaOH (0.5 M). Then, the final pH of each flask was measured, followed by the addition of 1 g photo-electrode under severe agitation after 24 h. The pH differences at the beginning and at the end of 24 h should be plotted, and the intersection point on the curve would be the pH_{zpc}[24].

Experimental analysis of variables

The pH of the various required solutions was analyzed by a digital pH meter (HACH, Model HQ411D). Important parameters wastewater characterization including chemical oxygen demand (COD), total dissolved solids (TDS), biochemical oxygen demand (BOD_5), and total suspended solids (TSS) were determined according to standard methods for examination of water and wastewater[25]. Evaluation of total organic carbon (TOC) was carried out by A TOC analyzer (Shimadzu, Japan) to investigate the mineralization rate of organics.

For measurement of RB19 after each experimental run, 15 mL desired sample was withdrawn and centrifuged at 5000 rpm for 5 min to separate any possible solid particle. Stability of photo-electrodes was evaluated through weighting of the electrode mass before and after the reaction followed by dryness at 103 °C. The residual concentration of RB19 was quantified with a spectrophotometer (Hach, DR 5000, USA) at the maximum wavelength of 590 nm[26]. The removal (%) was calculated according to Eq. (1):

$$Removal\,(\%) = \frac{C_0 - C_t}{C_0} \times 100 \tag{1}$$

where C_0 and C_t are the RB19 concentration and initial and desired reaction time, respectively.

Toxicity assessment using oxygen consumption rate inhibition (OCRI) test

The calculation of oxygen consumption rate inhibition (OCRI) was conducted according to ISO 8192[27], with some modifications. A bacterial consortium of 4 g/L was prepared. The nutrient substrate was comprised of urea 3 g/L, beef extract 11 g/L, peptone 16 g/L, K_2HPO_4 2.8 g/L, NaCl 0.7 g/L, $CaCl_2{\cdot}2H_2O$ 0.4 g/L, $MgSO_4{\cdot}7H_2O$ 0.2 g/L, sodium acetate 90 mg/L. The aeration tube was filled with 10 mL of sample, 8 mL of bacterial seed, 1 mL of the nutrient substrate, and 1 mL of water. The mixture was then aerated for 30 min. The oxygen consumption rate was monitored using a respirator (Model: EZ7900 HACH, Germany). The OCRI was calculated using Eq. (2):

$$OCRI = \frac{D_0 - D_t}{D_0} \times 100 \tag{2}$$

where D_0 and D_t are the oxygen consumption rate of the control and test groups, respectively.

Results and discussion

Photoelectrode characterization

The FESEM images of BG, BTN, and GBPE can be observed in Fig. 1. Figure 1b demonstrated the spherical morphology of BTN, which this character was remained finally after the modification of the surface of BG sheets to synthetize the photo electrode. In addition, the nano-sized diameter of BT in the range of 56–78 nm was proved according to Fig. 1b. As can be seen from Fig. 1c, BTN were well dispersed with an almost high coverage on the surface of BG sheets to form a GBPE which later will be proved with XRD patterns. In synthesis of composites, small agglomerations are anticipated which makes difference in estimation the size of particles between different analytical techniques such as SEM images and the Debye–Scherrer equation in XRD analysis[28]. Also, the EDS analysis revealed the elemental composition of BT, BG, and GBPE which proved the indicated the high purity of the synthetized nanoparticles and composite due to the major presence of carbon and titanium.

Figure 2 indicates the XRD patterns of BG, BTN, and GBPE. The standard card number JCPDS 00-008-0415 was used for verification of the main dominant peaks of carbon at 2θ of 20.19°, confirming the graphite structure in the composite as can be seen in Fig. 2a. The standard card number JCPDS 01-084-1750 was used to compare the observed peaks of BTN for verification of TiO_2 synthesis. According to Fig. 2b, sharp peaks of BTN were placed at 2θ of 25.39°, 38.94°, 47.89°, 53.99°, 55.12°, 62.54°, 68.36°, 71.48°, 74.89° and 75.92 which correspond to diffractions of TiO_2 nanoparticles[29], as a clear sign of efficient synthesis of BTN. It should be noted that, the BTN demonstrated a crystalline size of 40–65 nm according to Scherer's equation (Eq. 3). This data was in agreement with our previous work[30].

$$D = \frac{0.9\lambda}{\beta \cos\theta} \tag{3}$$

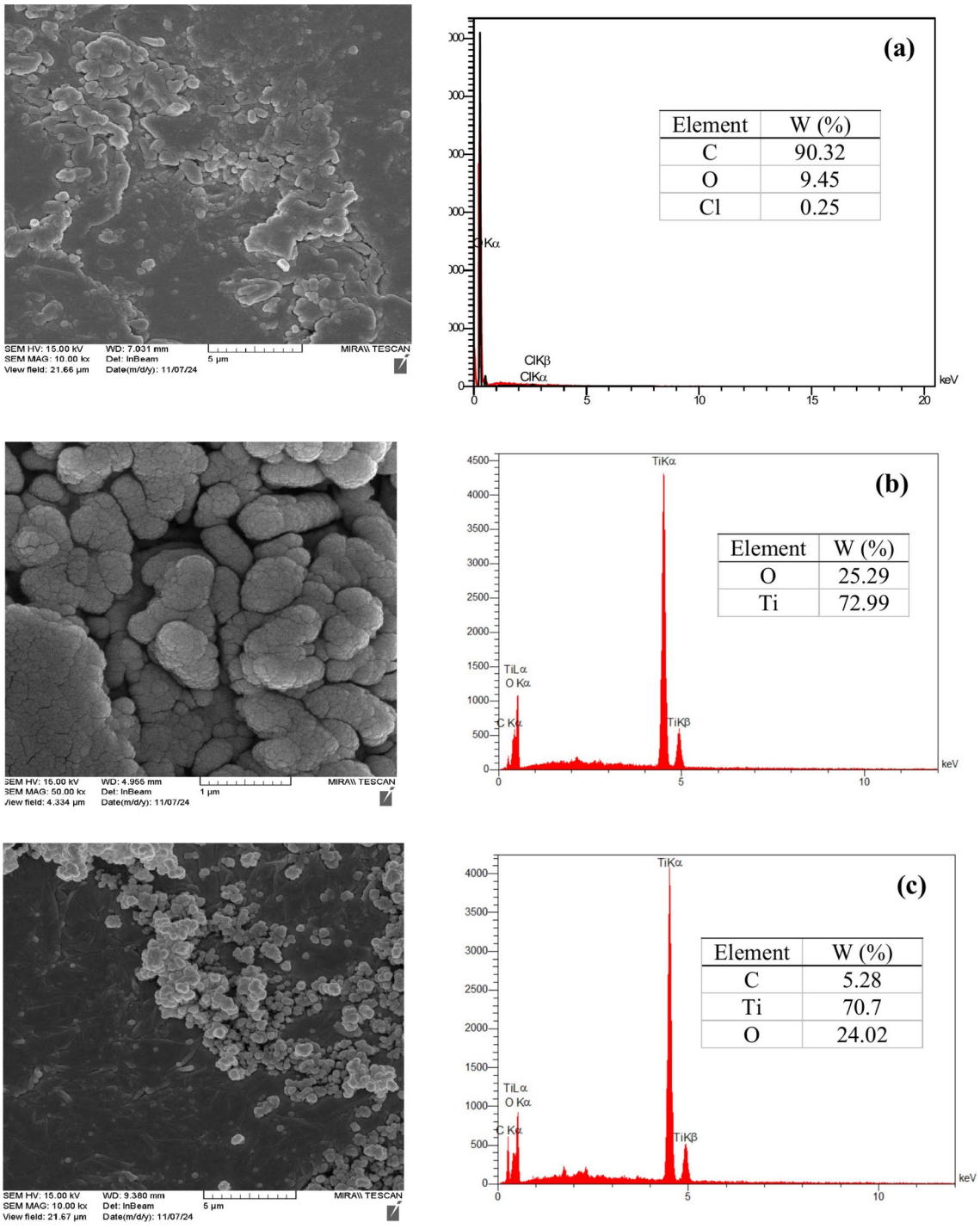

Fig. 1. SEM images of (**a**) BG, (**b**) BTN, (**c**) GBPE, along with corresponding EDS micrographs and (**d**) the histogram graph of TiO_2 nanoparticles.

The XRD patterns in Fig. 2c also show the successful attachment of BTN on the surface of BG, which proves the observation of the carbon XRD spectra simultaneously, indicating the successful synthesis of the photo-electrode using BTN and BG as the base. The GBPE showed several sharp peaks at 2θ of 26.49 (carbon, JCPDS 00-008-0415), and 37.86, 38.68, 48.13, 54.02, 62.88, 68.99, 70.51 and 75.32 which were belonged to TiO_2 (JCPDS 01-073-1764). Therefore, it can be concluded that that BTN were not destroyed during the synthesis of composite and desired photo-electrode is produced.

Figure 3 demonstrates the Fourier transform-infrared (FTIR) spectra of GBPE. The peaks at 1630, and 2923, 2360 cm^{-1} were associated with the C=C and C–H stretching vibrations for graphite, synthesized BTN and GBPE, respectively. The peak at 1630 cm^{-1} may be due to the interaction between graphite and TiO_2 nanoparticles in

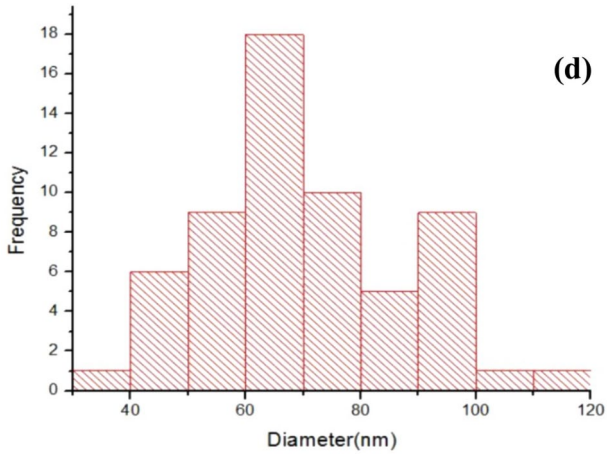

Figure 1. (continued)

the modified sample. Vibrations in the Ti-O-Ti network, also appeared on a band centered at 1131 and 977 cm^{-1}, suggesting the presence of TiO_2 nanoparticles in the electrode structure.

Photo-electrokinetic oxidation

Effect of pH

Figure 4 demonstrates the effect of the initial pH on RB19 removal using constant voltage value of 0.5V, reaction time of 20 min, UVA intensity of 12 W and RB19 concentration of 100 mg/L. Acidic pH values favored the RB19 removal up to pH 5 and removal efficiencies of as high as 33 ± 2.2% were obtained in 20 min. The photo-oxidation of many synthetic pollutants like dyes is highly pH dependent. In such reactions, the solution pH affects both the surface properties of the photo-electrode and the surface charge of the contaminant. Two kinds of basic reactions including photo-oxidation and electrolysis happen simultaneously.

Electrolysis of water using graphite electrodes produces H^+ and OH^- ions that a pH gradient would be created accordingly[31]. Furthermore, H_2O_2 would be generated according to Eqs. (4 & 5). Modification of cathode surface with TiO_2 nanoparticles along with production of H_2O_2 in presence of UVA irradiation provides a photo-oxidation reaction as a proved advanced oxidation process leading to production of highly reactant radicals, especially $OH^{\cdot}$, which related reactions are provided in Eqs. (4–9).

Another fact for better performance of the reaction system in acidic pHs can be related to most effective production of $OH^{\cdot}$ in acidic pH as the main oxidative spice of photo-oxidation reactions using TiO_2 nanoparticles[32]. Since electrolysis is one the two basic reactions in reaction chamber and is highly electrolyte dependent, higher pH values would consume the electrolyte excessively and in turn adversely affects the reaction efficiency through reduction of the solution conductivity. In addition, it should be noted that H^+ ions prevent the decomposition of $OH^{\cdot}$ under acidic conditions[33,34].

$$OH^{\cdot} + H_2O_2 \rightarrow HO_2 + H_2O^{\cdot} \tag{4}$$

$$OH^{\cdot} + OH^{\cdot} \rightarrow H_2O_2 \tag{5}$$

$$PE \xrightarrow{\lambda} GBPE\left(e_{cb}^{-} + h_{vb}^{+}\right). \tag{6}$$

$$GBPE\left(e_{cb}^{-} + h_{vb}^{+}\right) \rightarrow G\left(h_{VB}^{+} + TiO_2\left(e_{CB}^{-}\right)\right) \tag{7}$$

$$TiO_2\left(e_{CB}^{-}\right) + (O_2) \rightarrow TiO_2 + \left(O_2^{-}\right) \tag{8}$$

$$TiO_2\left(h_{VB}^{-/+}\right) + (OH)_{ads}^{-} \rightarrow TiO_2 + (OH)_{ads}^{\cdot} \tag{9}$$

The pH of the solution significantly affects the surface charge of both the photo-electrode and the dye molecule. At acidic pH, the GBPE surface becomes more positively charged, enhancing adsorption of RB19 dye onto the electrode surface via electrostatic attraction. According to results, at pH values of higher than 5, the efficiency decreased due to reduced adsorption and the excessive consumption of electrolyte, which reduces the overall reaction efficiency.

Apart from the reaction system, the structure of the pollutant also plays an important role in degradation efficiency in relation to solution pH. In this regard, the point of zero charge (pH_{zpc}), the pH at which the net charge of specified target is equal to zero, should be determined. The surface of the material is negatively charged when the pH is higher than pH_{zpc} and positively charged when pH is lower than pH_{zpc}. There is no electrical charge at the material surface at pH_{zpc}, or the surface of material is neutral. The pH_{zpc} for synthetized photo-electrode (graphite + TiO_2 nanoparticles) was 5.2 as determined in current work. Adsorption of a contaminant with a positive charge occurs when the pH of the solution is higher than pH_{zpc}, and vice versa. Since the RB19 is

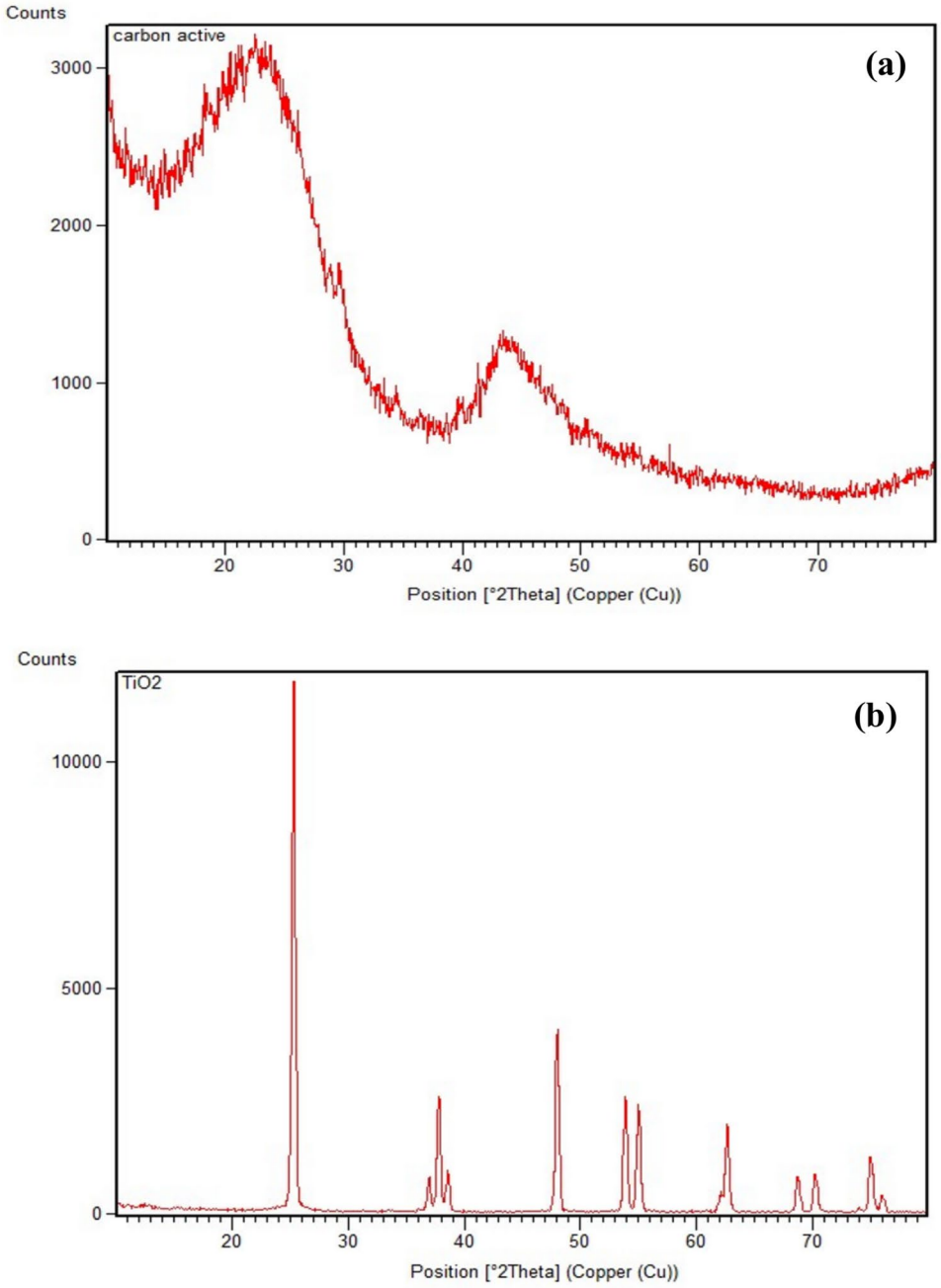

Fig. 2. XRD patterns of (**a**) BG, (**b**) BTN, (**c**) GBPE, and (**d**) plot of identified phases.

in an anionic color, the most efficient absorption on the surface of photo-electrode occurs when the pH is lower than 5.2. As can be seen from Fig. 4 the removal efficiency of RB19 decreased sharply in basic pH.

Effect UVA irradiation

Effect of UVA light irradiation on process efficiency was examined under the same reaction conditions as stated in "Effect of pH" section, but the pH level was fixed on 5 according to the obtained results of RB19 removal. Results indicated that with decreasing the UVA irradiation from 12 to 8 W and 4 W, the RB19 removal decreased to 28 ± 1.95% and 17 ± 3.05% respectively (Fig. 5). UVA irradiation enhances the generation of $HO^{\cdot}$ radicals through. The sorption of UVA irradiation by TiO_2 NPs stabilized on the graphite surface, produces excited electrons that subsequently transfers to the conduction band of TiO_2 NPs. The diffusion of the e^-/h^+ pairs to the surface of TiO_2 NPs is more effective than their recombination. If molecular oxygen is accessible in the solution, then the excited e^- at the surface of TiO_2 NPs reduces the O_2 to form the superoxide radical. Also, the e^- of the valance band of TiO_2 participate in generation of positive holes, which finally produce $HO^{\cdot}$ radicals through oxidation OH^-. Equations (10), (11), (13) demonstrate the summary of reactions leading to formation of $HO^{\cdot}$ radicals. It should be noted that in low UVA irradiation, the rate of H_2O_2 photolysis would be decreased

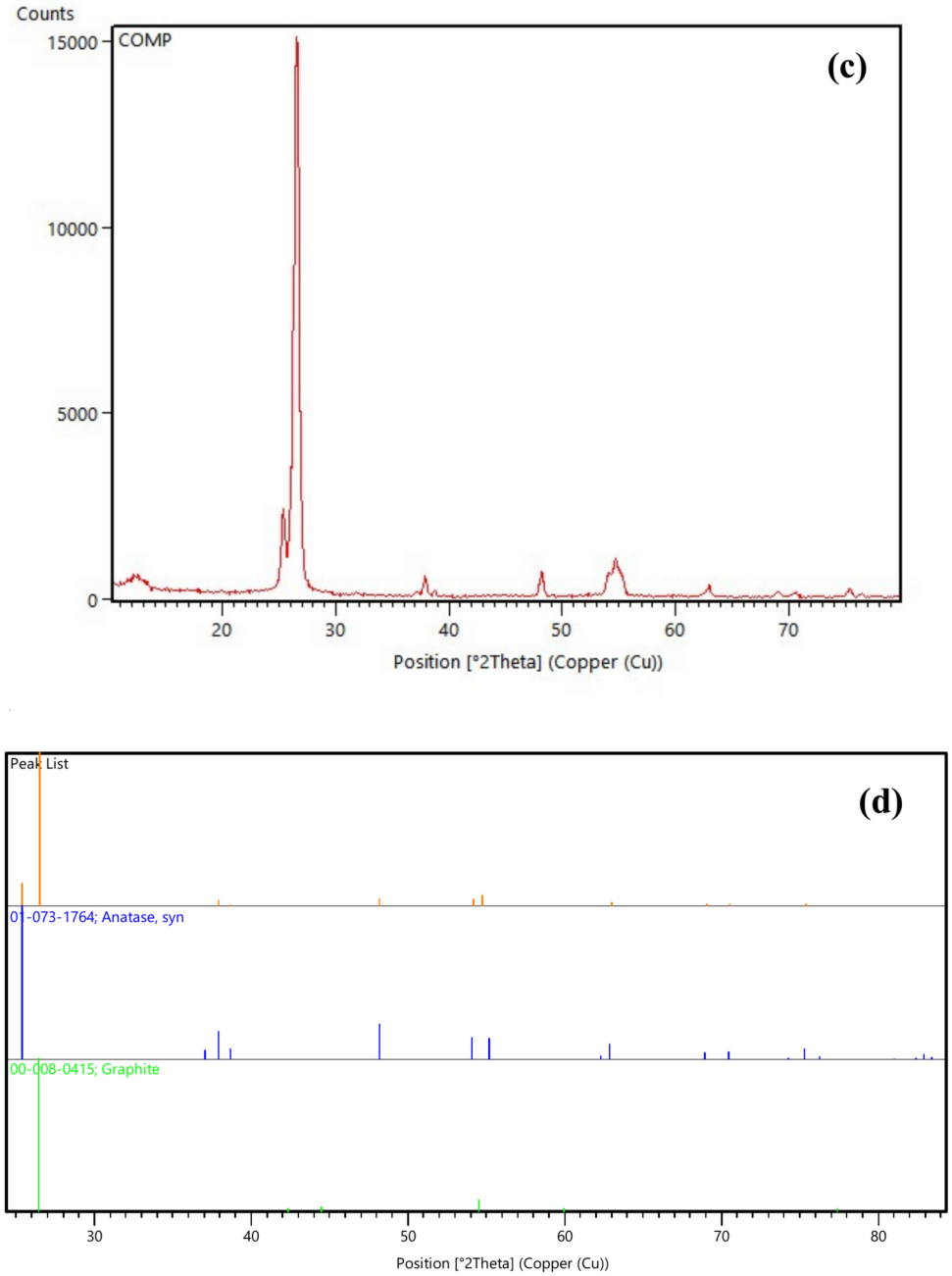

Figure 2. (continued)

which in turn affects the RB19 degradation adversely. Considering the significant influence of high levels of the UVA irradiation on RB19 degradation with corresponding removal rate of 33%, the UVA intensity of 12 W was selected for remaining experiments.

$$\mathrm{TiO_2} \xrightarrow{\lambda} \mathrm{TiO_2}\left(e^-_{\mathrm{cb}} + h^+_{\mathrm{vb}}\right) \tag{10}$$

$$\mathrm{TiO_2}\left(e^-_{\mathrm{cb}} + h^+_{\mathrm{vb}}\right) \rightarrow h^+_{\mathrm{vb}} + \mathrm{TiO_2}\left(e^-_{\mathrm{cb}}\right) \tag{11}$$

$$\mathrm{TiO_2}\left(e^-_{\mathrm{cb}}\right) + (\mathrm{O_2})_{\mathrm{ads}} \rightarrow \mathrm{TiO_2} + \left(\mathrm{O_2^-}\right) \tag{12}$$

$$\mathrm{TiO_2}\left(h^{-/+}_{\mathrm{vb}}\right) + (\mathrm{OH})^-_{\mathrm{ads}} \rightarrow \mathrm{TiO_2} + (\mathrm{OH})^{\cdot}_{\mathrm{ads}} \tag{13}$$

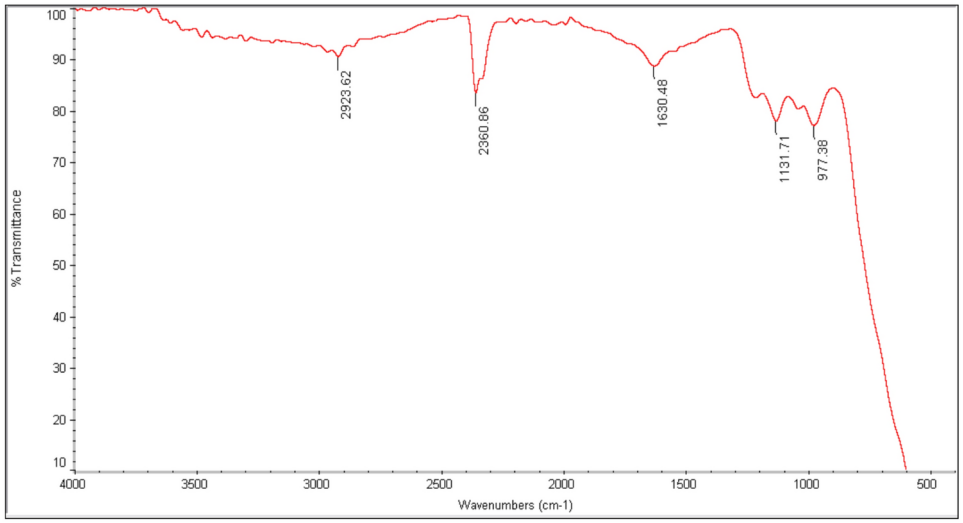

Fig. 3. FTIR spectra for GBPE.

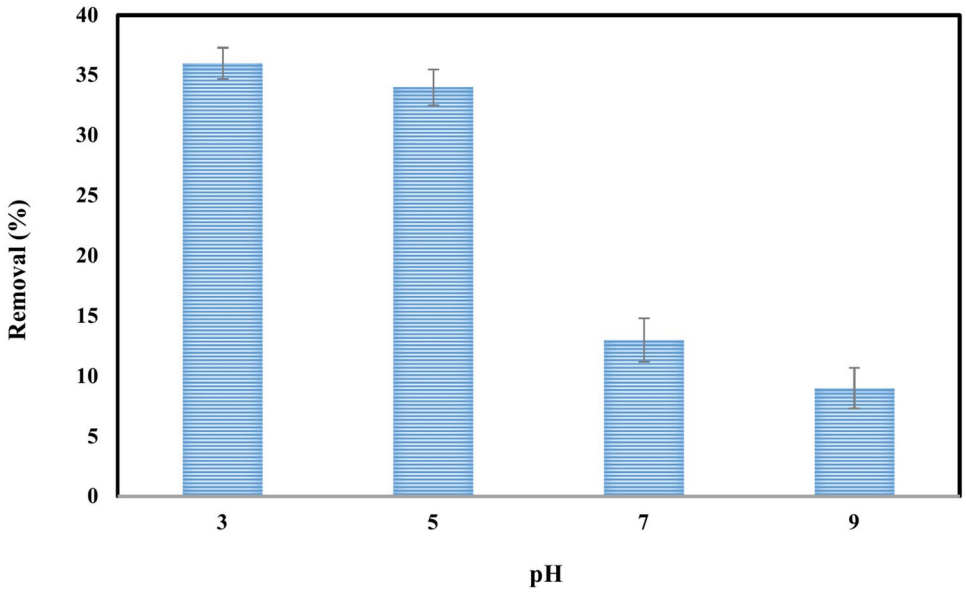

Fig. 4. Effect of pH in oxidation of RB19 using GBPE under UVA irradiation in an electrokinetic oxidation system (RB19: 100 mg/L, Reaction time: 20 min, Voltage: 0.5 V/cm, UVA: 12 W).

Effect of voltage and stability of electrodes

The voltage is known as an important and effective variable in electrochemical based reactions for degradation recalcitrant organic pollutants. Evaluation of the effect of voltage and stability of the electrodes in removal of RB19 were performed in predetermined conditions including pH 5, UVA irradiation of 12 W, RB19 concentration of 100 mg/L and at different time intervals in the range of 20–120 min. The RB19 removal raised proportional to the voltage and reached the maximum removal of 100% in voltage of 1.5 V/cm at 120 min, in voltage 2 V/cm at 100 min and voltages of 2.5 and 3 V/cm at 80 min. Simultaneously, the weight of electrodes was measured in all runs to analyze the stability of electrodes under varying voltages. As can be seen from data presented in Fig. 6, increasing the voltage, affects the stability of electrode in a reverse status and decreases the electrode weight. Higher voltages demonstrated rapid corrosion and weight decrease so that significant weigh removals (g) of 1.2, 2.1 and 2.9 were observed ate voltage values of 2, 2.5 and 3 V/cm, respectively. According to results presented at Figs. 6 and 7, the reaction contact time of 120 min at voltage of 1.5 V/cm led to maximum RB19 removal of 100% and was selected for remaining experiments. These obtained findings can be ascribed to this fact that in higher voltages and therefore higher current intensities the anodic oxidation of RB19 would be enhanced due to high generation rate of oxidizing agents such as hypochlorite and chlorine as well as hydrogen peroxide[35]. In addition,

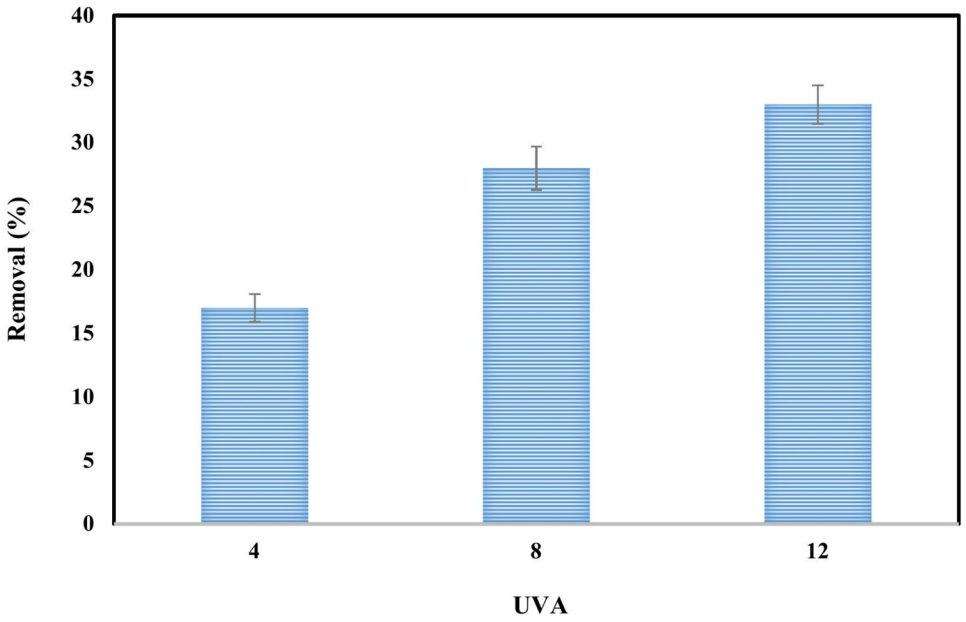

Fig. 5. Effect of UVA irradiation in oxidation of RB19 using GBPE under UVA irradiation in an electrokinetic oxidation system (RB19: 100 mg/L, Reaction time: 20 min, Voltage: 0.5 V/cm, pH: 5).

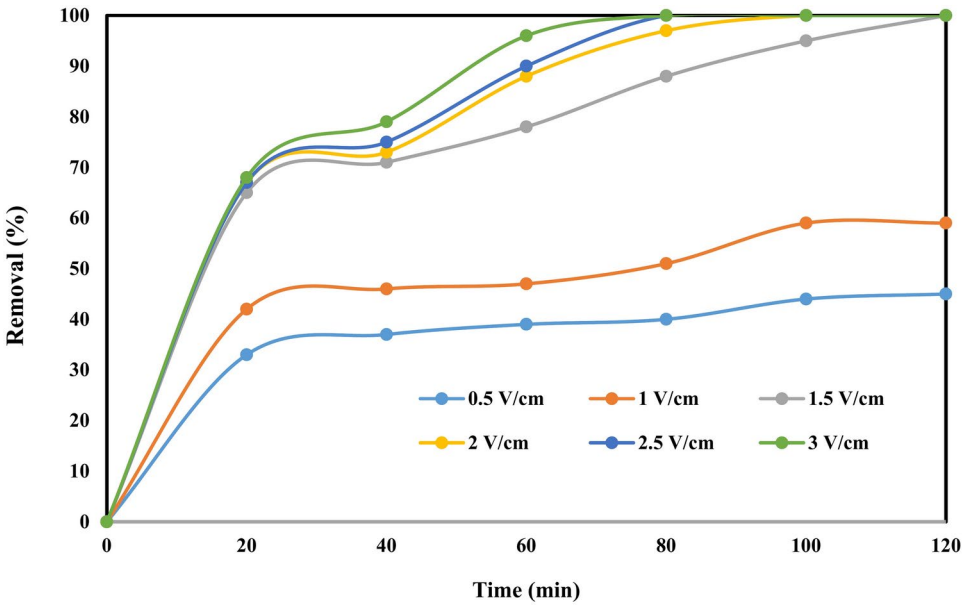

Fig. 6. Effect of voltage in oxidation of RB19 using GBPE under UVA irradiation in an electrokinetic oxidation system (RB19: 100 mg/L, UVA irradiation of 12 W, pH: 5).

the generation rate of $HO^{\cdot}$ radicals on the side of anode electrode increases significantly in higher voltages, in which production of more electrons, improves the reaction rate[36].

Removal mechanism of RB19 dye using GBPE

Reactive Blue 19 dye has a complex structure with azo bonds (N=N), which are typically the sites where degradation occurs. The reactive oxygen species (ROS) attack these bonds, breaking them and fragmenting the dye molecule into smaller intermediates and ultimately mineralize it into CO_2 and H_2O. The process involves both photocatalysis and electrochemical oxidation.

In the electrochemical reactions, chloride ions (Cl^-) are continuously oxidized at the anode to form chlorine gas (Cl_2) (Eq. 14) and various oxychlorine species such as hypochlorous acid/hypochlorite ($HOCl/OCl^-$),

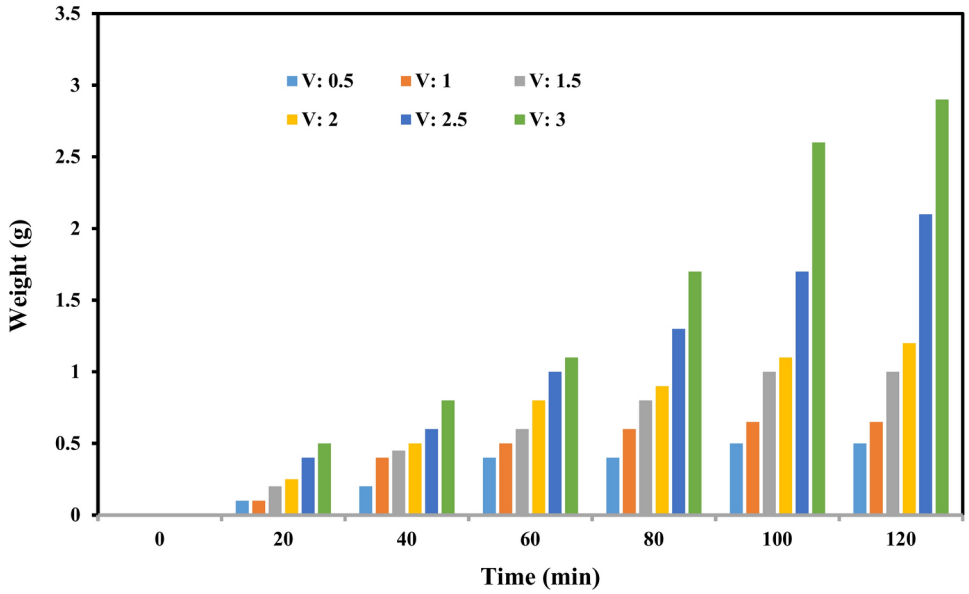

Fig. 7. Effect of voltage in stability of electrodes for oxidation of RB19 using GBPE under UVA irradiation in an electrokinetic oxidation system (RB19: 100 mg/L, UVA irradiation of 12 W, pH: 5).

chlorite (ClO_2^-), chlorate (ClO_3^-), and perchlorate (ClO_4^-) (Eq. 15)[37]. Additionally, Cl^- ions interact with hydroxyl radicals ($OH^{\cdot}$), generated at the graphite anode, to produce chlorine radicals (Eqs. 16 and 17)[38].

$$2Cl^- \rightarrow Cl_2 + 2e^- \tag{14}$$

$$Cl^- \rightarrow HOCl/OCl^- \rightarrow ClO_2^- \rightarrow ClO_3^- \rightarrow ClO_4^- \tag{15}$$

$$Cl^- \rightarrow HO^{\cdot} \Leftrightarrow HOCl^- \Leftrightarrow Cl^{\cdot} + OH^- \tag{16}$$

$$Cl^- + Cl^{\cdot} \Leftrightarrow Cl_2^- \tag{17}$$

The dye molecules are adsorbed onto the porous surface of GBPE electrode due to electrostatic interactions and π-π stacking between the dye's aromatic rings and the graphite structure. In the photocatalytic oxidation, the GBPE play a crucial role in the reaction. Upon GBPE exposure to UVA light, the dye degradation in the solution would be initiated by exciting electrons (e^-), which were subsequently transferred from the TiO_2's valence band (VB) to the conduction band (CB), creating electron–hole pairs (h^+). The graphite component, as an electron sink, facilitates the transfer of electrons from TiO_2 to its conductive surface, reducing recombination. In the presence of molecular oxygen (O_2), the excited electron on the GBPE interacts with oxygen, generating superoxide radicals ($^{\cdot}O_2^-$). This process highlights that the primary mechanism driving the reaction is the diffusion of electron–hole pairs, rather than their recombination. Electrons from the valence band of TiO_2 move towards the graphite surface, forming positive holes. The holes in the valence band can oxidize hydroxyl ions (OH^-) and lead to hydroxyl radicals ($OH^{\cdot}$) generation. Generated ROS ($^{\cdot}O_2^-$, $OH^{\cdot}$) attack the dye molecules, breaking the azo bonds and other functional groups of RB19. The fragmented molecules are further oxidized to simple, non-toxic compounds. At the end of the photocatalytic degradation, the dye molecules are broken down into carbon dioxide (CO_2), and water (H_2O).

According to Eqs. (18–22), the dye degradation can be attributed to the aggressive action of these radicals.

$$GBPE \xrightarrow{\lambda} GBPE\left(e_{cb}^- + h_{vb}^+\right) \tag{18}$$

$$GBPE\left(e_{cb}^- + h_{vb}^+\right) \rightarrow G\left(h_{VB}^+ + TiO_2\left(e_{CB}^-\right)\right) \tag{19}$$

$$TiO_2\left(e_{CB}^-\right) + (O_2) \rightarrow TiO_2 + \left(O_2^-\right) \tag{20}$$

$$TiO_2\left(h_{VB}^{-/+}\right) + (OH)_{ads}^- \rightarrow TiO_2 + (OH)_{ads}^{\cdot} \tag{21}$$

$$(OH)_{ads}^{\cdot} + RB19 \rightarrow Intermediate + CO_2 + H_2O \tag{22}$$

Alternative processes and electrode stability

The effect of stabilization of TiO_2 NPs on the function of photo-electrode on RB19 removal was studied and compared with in series of control experiments the same pre-determined conditions including the initial RB19

concentration of 100 mg/L, pH 5, and irradiation intensity of 12 W and voltage of 1.5 V/cm. The contact time for all experiments was set on 120 min and results can be found in Fig. 8.

The GBPE oxidation as yielded the maximum removal of 100% in intended time of 120 min. UVA irradiation along with EK oxidation demonstrated less performance in the same conditions with RB19 removal of 74%. The lower removal efficiency is certainly due to absence of TiO_2 nanoparticles and missing the capability of photocatalysit based reactions. The higher removal of RB19 can be attributed to the simultaneous participation of the adsorption, EK oxidation and photocatalytic degradation processes in the system. The EK oxidation alone and PC (photocatalytic) oxidation were also demonstrated considerable removals of 74% and 59% that reveals that both processes alone, demonstrate lower oxidation potential. In addition, the electrode stability of BG showed a significant decrease compared to GBPE in the same conditions.

The loose of graphite duo to corrosion was 1 g in GBPE which increased to 2.1 g in UVA/EK. This can be attributed to the fact that the main oxidation route in alternative number 2 was through EK oxidation and applying the electrical current on graphite. Results also indicated that stabilization TiO_2 on graphite sheet without light irradiation do not show any catalytic activity, but improves the graphite stability, since the electrode loose of 2.2 g in TiO_2/EK process was less than the graphite loose of 2.6 g in EK process in the same condition (Fig. 8). The protecting role of TiO_2 stabilization on the surface of graphite needs to be investigated and was a suppressing finding in current study.

Reusability is an important issue for modified electrodes. In this study, stability of TNPs on GBPE was investigated by a series of successive experiments. Cleaning of the graphite electrode surface was carried out after each run with deoxygenated distilled water and ethanol to remove any residual derby from pervious experiment, and then dried in oven at 80 °C for 24 h to be ready for the next experimental run. As can be seen from Fig. 9, the removal efficiency of RB19 at the end of sixth run decreased to 63%, indicating the loose of catalytic activity after each reaction run due to removal and washout of some of stabilized TNPs.

Toxicity assessment using OCRI test

Results of toxicity of final effluent of UVA/TNPs/EK oxidation process for degradation of RB19 are presented in Fig. 10. Results of OCRI test showed a decrease in toxicity in the order of highest to lowest for EK, UVA/EK and UVA/TNPs/EK. The trends of toxicity evaluation agree with the removal rates.

Real wastewater treatment

Characteristics of real textile wastewater for performing a set of experiments in desired conditions can be shown in Table 1. The removal efficiencies of 32% and 40% were observed for initial COD and TOC concentrations of 1284 mg/L and 912 mg/L respectively, using enhanced electrolysis with GBPE in pH equal to 5, voltage of 1.5 V/cm and the reaction time of 120 min. Results can be observed in Table 2. Advanced oxidation processes including electrokinetic based reactions such as enhanced electrolysis are characterized by fast partial oxidation and long-term mineralization of intermediates. Therefore, despite of almost low COD and TOC removal efficiencies, it can be concluded that the heavy and big molecules of different pollutants in textile effluents, are subjected to some oxidation, but the final mineralization has not been achieved yet[37], and more reaction time would be required.

Various processes have used for textile wastewater treatment. In performed study on suspended photocatalytic treatment for textile effluent with total COD of 370 mg/L, COD removal of 45% and 23% were obtained using TiO_2 and ZnO catalysts during 3 h UV-A lamp irradiation[39]. In our study, the use of TiO_2/Graphite (GBPE)

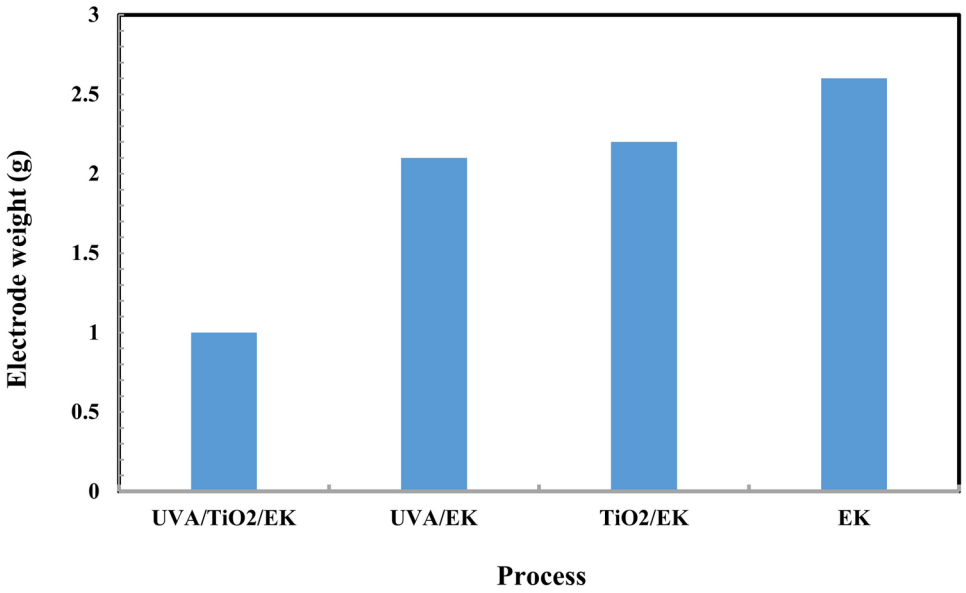

Fig. 8. Weight loose of graphite sheet in different alternative processes in the same reaction conditions (RB19: 100 mg/L, UVA irradiation: 12 W, pH: 5, voltage: 1.5 V/cm, reaction time: 120 min).

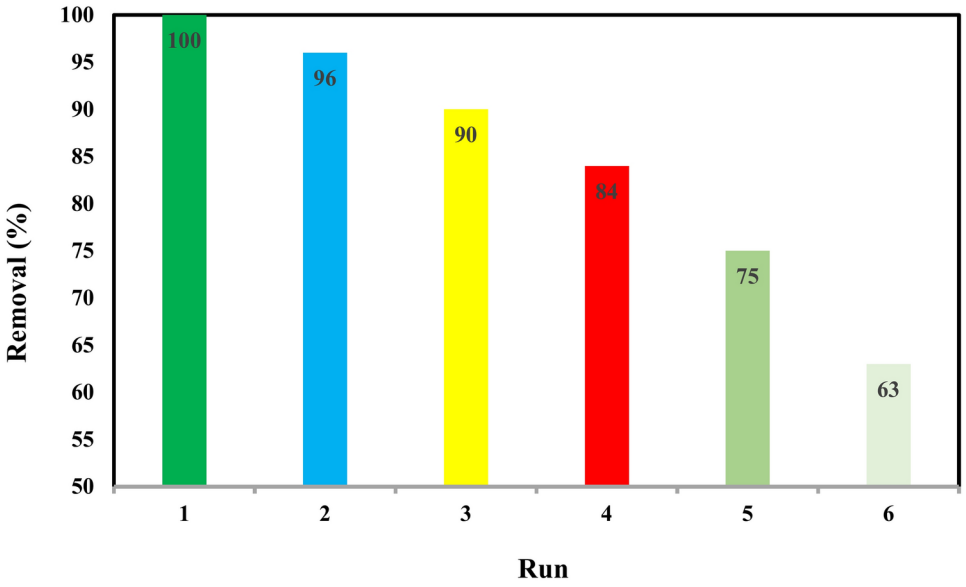

Fig. 9. Reusability of GBPE during UVA/TNPs/EK oxidation of RB19 under selected conditions (pH: 5, voltage: 1.5 V/cm, reaction time: 120 min, UVA: 12 W, RB19: 100 mg/L).

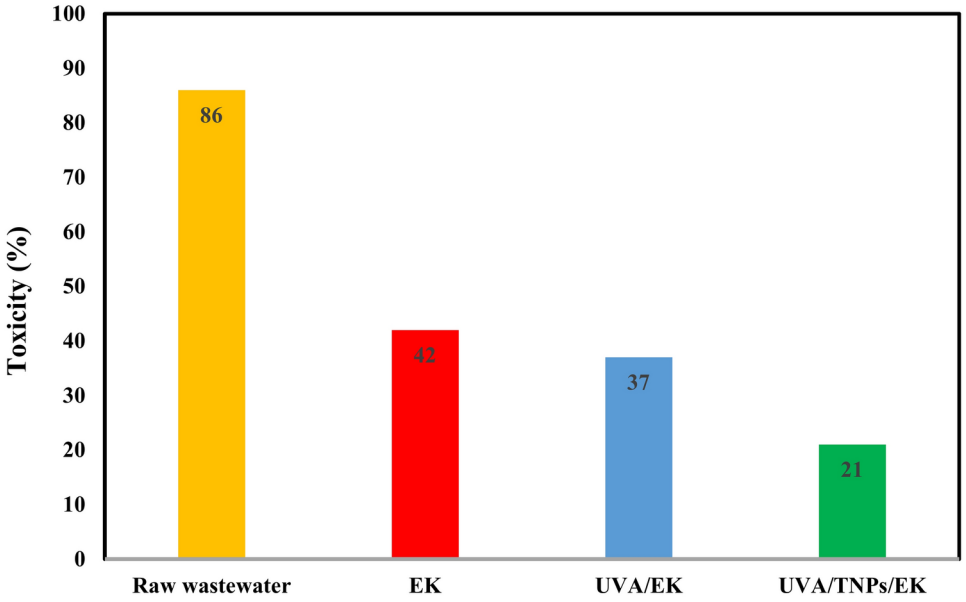

Fig. 10. Results of toxicity assessment using OCRI for raw and treated solutions.

Parameter	Raw wastewater	Reaction time		
		30 min	60 min	120 min
Total COD (mg/L)	1284	1038	924	873
TOC (mg/L)	912	830	782	547

Table 2. The COD and TOC removal in electrokinetic oxidation process using GBPE for treatment of real textile wastewater (pH: 5, reaction time 12 min, voltage of 1.5 V/cm, UVA: 12 W).

photoelectrode increases the stability of the electrode while simultaneously performing photocatalytic and electrochemical decomposition.

Conclusion

The treatment of textile wastewater, which often contains toxic dyes like RB19, is a environmental challenge. Photo-electrochemical (PEC) processes have been widely explored as effective processes due to their ability to combine photocatalytic degradation with electrochemical oxidation. This study aimed to synthesize and evaluate titanium/graphite composite photo-electrode (GBPE) under varying voltages for textile wastewater treatment using RB19 as a model contaminant.

According to the results, the highest removal efficiency of RB19 occurred under acidic pH conditions. The applied voltage in photo-electrokinetic systems plays a critical role in the dye degradation. In the present study, 100% removal efficiency was achieved at various voltages and reaction times. Adding protective layers, such as carbon-based coatings (e.g., graphite layers) can protect the electrode from corrosion, and improve stability at higher voltages. Based on the results, a voltage of 1.5 V/cm with a reaction time of 120 min was selected as the optimum value.

According to the results, TiO_2 immobilized on GE without light irradiation showed no catalytic activity. The removal efficiency of RB19 after sixth run decreased to 63%, indicating the loss of catalytic activity due to removal and washout of stabilized NPs after each reaction run. The OCRI test results revealed that the highest and lowest of reduction in toxicity was related to UVA/TNPs/EK and EK processes, respectively.

Generally, the findings suggest that GBPE can be used as an effective photoelectrode for the removal of RB19 dye as a model pollutant from aqueous solutions. Investigation of real textile wastewater using enhanced electrolysis with GBPE showed the removal efficiencies of 32% and 40% for COD and TOC, respectively. However, complete mineralization has not been achieved yet, indicating the need for more reaction times. Further research into electrode modification and the performance of PEC processes are recommended to improve and practical application of this technology in wastewater treatment. We propose future research directions such as improving the reusability of the electrodes, optimizing reaction times, and exploring other types of real wastewater to further assess the applicability of this composite in practical applications.

Data availability

All data generated or analysed during this study are included in this published article.

Received: 25 January 2025; Accepted: 7 April 2025
Published online: 25 April 2025

References

1. Azanaw, A., Birlie, B., Teshome, B. & Jemberie, M. Textile effluent treatment methods and eco-friendly resolution of textile wastewater. *Case Stud. Chem. Environ. Eng.*. **6**, 100230 (2022).
2. Castillo-Suárez, L. A., Sierra-Sánchez, A. G., Linares-Hernández, I., Martínez-Miranda, V. & Teutli-Sequeira, E. A. A critical review of textile industry wastewater: Green technologies for the removal of indigo dyes. *Int. J. Environ. Sci. Technol. (Tehran)* **20**, 1–38 (2023).
3. Al-Tohamy, R. et al. A critical review on the treatment of dye-containing wastewater: Ecotoxicological and health concerns of textile dyes and possible remediation approaches for environmental safety. *Ecotoxicol. Environ. Saf.* **231**, 113160 (2022).
4. Mehra, S., Singh, M. & Chadha, P. Adverse impact of textile dyes on the aquatic environment as well as on human beings. *Toxicol. Int.* **28**, 165 (2021).
5. Le Luu, T. & Ngan, P. T. K. Fabrication of high performance Ti/SnO_2-Nb_2O_5 electrodes for electrochemical textile wastewater treatment. *Sci. Total Environ.* **860**, 160366 (2023).
6. Rathinam, R. & Govindaraj, M. Photoelectrocatalytic oxidation of textile industry wastewater by RuO_2/IrO_2/TaO_2 coated titanium electrodes. *Nat. Environ. Pollut. Technol.* **20**, 1069 (2021).
7. Sehar, S. et al. Recent advances in biodecolorization and biodegradation of environmental threatening textile finishing dyes. *3 Biotech.* **12**, 186 (2022).
8. Zhang, Y., Shaad, K., Vollmer, D. & Ma, C. Treatment of textile wastewater using advanced oxidation processes—a critical review. *Water* **13**, 3515 (2021).
9. Rajasimman, M., Babu, S. V. & Rajamohan, N. Biodegradation of textile dyeing industry wastewater using modified anaerobic sequential batch reactor–start-up, parameter optimization and performance analysis. *J. Taiwan Inst. Chem. Eng.* **72**, 171–181 (2017).
10. Asfaram, A., Ghaedi, M., Ghezelbash, G. R. & Pepe, F. Application of experimental design and derivative spectrophotometry methods in optimization and analysis of biosorption of binary mixtures of basic dyes from aqueous solutions. *Ecotoxicol. Environ. Saf.* **139**, 219–227 (2017).
11. Suhadolnik, L. et al. Continuous photocatalytic, electrocatalytic and photo-electrocatalytic degradation of a reactive textile dye for wastewater-treatment processes: Batch, microreactor and scaled-up operation. *J. Ind. Eng. Chem.* **72**, 178–188 (2019).
12. Umukoro, E. H., Peleyeju, M. G., Ngila, J. C. & Arotiba, O. A. Towards wastewater treatment: Photo-assisted electrochemical degradation of 2-nitrophenol and orange II dye at a tungsten trioxide-exfoliated graphite composite electrode. *Chem. Eng. J.* **317**, 290–301 (2017).
13. Singaravadivel, C., Vanitha, M. & Balasubramanian, N. Photo and electrocatalytic treatment of textile wastewater and its comparison. *J. Electrochem. Sci. Technol.* **3**, 44–49 (2012).
14. Ramli, Z. A. C. et al. Photocatalytic degradation of methylene blue under UV light irradiation on prepared carbonaceous TiO_2. *Sci. World J.* **2014**, 415136 (2014).
15. Vaez, M., Zarringhalam Moghaddam, A. & Alijani, S. Optimization and modeling of photocatalytic degradation of azo dye using a response surface methodology (RSM) based on the central composite design with immobilized titania nanoparticles. *Ind. Eng. Chem. Res.* **51**, 4199–4207 (2012).
16. Nguyen, C. H., Tran, M. L., Tran, T. T. V. & Juang, R.-S. Enhanced removal of various dyes from aqueous solutions by UV and simulated solar photocatalysis over TiO_2/ZnO/rGO composites. *Sep. Purif. Technol.* **232**, 115962 (2020).
17. Ge, Y., Luo, H., Huang, J. & Zhang, Z. Visible-light-active TiO_2 photocatalyst for efficient photodegradation of organic dyes. *Opt. Mater.* **115**, 111058 (2021).

18. Akerdi, A. G., Bahrami, S. H. & Pajootan, E. Modeling and optimization of photocatalytic decolorization of binary dye solution using graphite electrode modified with Graphene oxide and TiO_2. *J. Environ. Health Sci. Eng.* **18**, 51–62 (2020).
19. Ama, O. M. & Arotiba, O. A. Exfoliated graphite/titanium dioxide for enhanced photoelectrochemical degradation of methylene blue dye under simulated visible light irradiation. *J. Electroanal. Chem.* **803**, 157–164 (2017).
20. Khataee, A. R., Safarpour, M., Zarei, M. & Aber, S. Combined heterogeneous and homogeneous photodegradation of a dye using immobilized TiO_2 nanophotocatalyst and modified graphite electrode with carbon nanotubes. *J. Mol. Catal. A Chem.* **363–364**, 58–68 (2012).
21. Khalid, N. R., Ahmed, E., Hong, Z., Sana, L. & Ahmed, M. Enhanced photocatalytic activity of graphene–TiO_2 composite under visible light irradiation. *Curr. Appl. Phys.* **13**, 659–663 (2013).
22. Zhang, H., Lv, X., Li, Y., Wang, Y. & Li, J. P25-graphene composite as a high performance photocatalyst. *ACS Nano* **4**, 380–386 (2010).
23. Nair, A. T., Makwana, A. R. & Ahammed, M. M. The use of response surface methodology for modelling and analysis of water and wastewater treatment processes: A review. *Water Sci. Technol.* **69**, 464–478 (2014).
24. Isari, A. A., Payan, A., Fattahi, M., Jorfi, S. & Kakavandi, B. Photocatalytic degradation of rhodamine B and real textile wastewater using Fe-doped TiO_2 anchored on reduced graphene oxide (Fe-TiO_2/rGO): Characterization and feasibility, mechanism and pathway studies. *Appl. Surf. Sci.* **462**, 549–564 (2018).
25. APHA. *Standard Methods for the Examination of Water and Wastewater*, 20 th edition. American Public Health Association, 2002. (2018).
26. Delnavaz, M., Farahbakhsh, J. & Mahdian, S. S. Photodegradation of reactive blue 19 dye using magnetic nanophotocatalyst α-Fe_2O_3/WO_3: A comparison study of α-Fe_2O_3/WO_3 and WO_3/NaOH. *Water Sci. Eng.* **14**, 119–128 (2021).
27. ISO, *Water Quality–Test for Inhibition of Oxygen Consumption by Activated Sludge for Carbonaceous and Ammonium Oxidation*. 2007, International Organization for Standardization Geneva.
28. Najafi, M., Kermanpur, A., Rahimipour, M. R. & Najafizadeh, A. Effect of TiO_2 morphology on structure of TiO_2-graphene oxide nanocomposite synthesized via a one-step hydrothermal method. *J. Alloy. Compd.* **722**, 272–277 (2017).
29. Fan, Z. et al. Enhanced photocatalytic activity of hierarchical flower-like CeO_2/TiO_2 heterostructures. *Mater. Lett.* **175**, 36–39 (2016).
30. Jorfi, S., Mirali, S., Mostoufi, A. & Ahmadi, M. Visible light photocatalytic degradation of azo dye and a real textile wastewater using Mn, Mo, La/TiO_2/AC nanocomposite. *Chem. Biochem. Eng. Q.* **32**, 215–227 (2018).
31. Acar, Y. B., Alshawabkeh, A. N. & Gale, R. J. Fundamentals of extracting species from soils by electrokinetics. *Waste Manage.* **13**, 141–151 (1993).
32. Dai, Q. et al. The application of a novel Ti/SnO_2–Sb_2O_3/PTFE-La-Ce-β-PbO_2 anode on the degradation of cationic gold yellow X-GL in sono-electrochemical oxidation system. *Sep. Purif. Technol.* **104**, 9–16 (2013).
33. Da Pozzo, A. et al. Removal of the herbicide amitrole from water by anodic oxidation and electro-Fenton. *Environ. Chem. Lett.* **3**, 7–11 (2005).
34. Laine, D. F. & Cheng, I. F. The destruction of organic pollutants under mild reaction conditions: A review. *Microchem. J.* **85**, 183–193 (2007).
35. da Silva Santana, I. L. et al. Electrodegradation of direct black 22 in textile effluents using graphite and copper electrodes. *Appl. Catal. O Open.* **188**, 206925 (2024).
36. Belal, R. M., Zayed, M. A., El-Sherif, R. M. & Abdel Ghany, N. A. Advanced electrochemical degradation of basic yellow 28 textile dye using IrO_2/Ti meshed electrode in different supporting electrolytes. *J. Electroanal. Chem.* **882**, 114979 (2021).
37. Jorfi, S., Pourfadakari, S. & Ahmadi, M. Electrokinetic treatment of high saline petrochemical wastewater: Evaluation and scale-up. *J. Environ. Manage.* **204**, 221–229 (2017).
38. da Silva, F. M., Orssatto, F., Leite, O. D., Falchi, M. L. & Gomes, B. M. Degradation of acid black 210 Na AZO dye through electro-oxidation with graphite electrodes. *Desalin. Water Treat.* **320**, 100717 (2024).
39. Çifçi, D. & Meriç, S. Optimization of suspended photocatalytic treatment of two biologically treated textile effluents using TiO_2 and ZnO catalysts. *Glob. NEST J.* **17**, 653–663 (2015).

Acknowledgements

This paper has been financially supported by Environmental Technologies Research Center, Ahvaz Jundishapur University of Medical Sciences [Grant number: ETRC 9912]. The issued ethical code is IR.AJUMS.REC.1399.667.

Author contributions

M.D.: Conceptualization, Investigation, Writing—original draft, Writing—review & editing. B.J: Investigation, Writing—original draft. S. J.: Project administration, Conceptualization, Formal analysis, Writing—original draft, Writing—review & editing. B.M. and A.B.: Investigation, Validation, Formal analysis.

Declarations

Competing interests

The authors declare no competing interests.

Additional information

Correspondence and requests for materials should be addressed to S.J.